Displacement Field-Controlled Fractional Chern Insulators and Charge Density Waves in a Graphene/hBN Moiré Superlattice

Samuel H. Aronson,[1,*] Tonghang Han,[1,*] Zhengguang Lu,[1] Yuxuan Yao,[1] Jackson P. Butler,[1] Kenji Watanabe,[2] Takashi Taniguchi,[3] Long Ju,[1,†] and Raymond C. Ashoori[1,‡]

[1]*Department of Physics, Massachusetts Institute of Technology, Cambridge, Massachusetts, USA*
[2]*Research Center for Electronic and Optical Materials, National Institute for Materials Science, Tsukuba, Japan*
[3]*Research Center for Materials Nanoarchitectonics, National Institute for Materials Science, Tsukuba, Japan*

(Received 15 January 2025; revised 17 April 2025; accepted 11 June 2025; published 24 July 2025)

Rhombohedral stacked graphene (RSG) contains two key ingredients for the realization of correlated topological phases of matter: flat electronic bands and concentrated Berry curvature. The fractional quantum anomalous Hall effect was recently observed in an RSG-hexagonal boron nitride (hBN) moiré heterostructure when the conduction electrons were pushed away from the moiré interface by an applied electric displacement field. The question then arises about whether such topological states can also develop in RSG-hBN in a strong moiré potential. Here, we explore the physics in the moiré-proximal limit through capacitance measurements that allow us to determine the electronic compressibility and extract energy gaps of incompressible states. We report the observation of integer and fractional Chern insulator states at low magnetic field in this limit at filling factors $\nu = 1$, $2/3$, and $1/3$ in addition to numerous trivial and topological charge density waves. We map out a correlated phase diagram that is highly sensitive to both displacement and magnetic fields, establishing the moiré-proximal regime as a tunable platform for studying the interplay between band topology and strong lattice effects.

DOI: 10.1103/75gl-jzl6 Subject Areas: Condensed Matter Physics

I. INTRODUCTION

In the presence of an external magnetic field, the continuous energy bands of a two-dimensional electron gas (2DEG) break up into discrete, highly degenerate Landau levels. When the chemical potential sits between Landau levels, the 2DEG exhibits the integer quantum Hall effect, in which the system has a bulk gap but supports dissipationless chiral edge modes and a Hall conductance quantized to an integer multiple of e^2/h [1]. At certain rational fillings of a Landau level, electronic correlations open up a gap in the many-body spectrum, leading to the fractional quantum Hall effect (FQHE) [2]. Flat, isolated Chern minibands in moiré materials are lattice analogs of the field-induced Landau levels required for conventional quantum Hall physics. In these bands, Berry curvature plays a role similar to that of an external magnetic field, while the narrow bandwidth quenches the electrons' kinetic energy, allowing electronic correlations to dominate the low-energy physics. When a Chern band is fully filled, the result is a Chern insulator (CI), a state which, like a conventional quantum Hall insulator, hosts dissipationless edge modes and quantized Hall conductance [3]. In analogy to correlations in a partially filled Landau level producing a fractional quantum Hall insulator, a partially filled Chern band can give rise to a fractional Chern insulator (FCI) [4–10].

Even though Chern bands have intrinsic topology, an external magnetic field is often required to induce FCI ground states [11,12]. However, recent experiments demonstrated the fractional quantum anomalous Hall effect (FQAHE), the zero-field counterpart to the FQHE, in two remarkably different systems. In twisted bilayer $MoTe_2$ [13–16], a strong superlattice potential generates flat, isolated moiré bands which are similar to Landau levels at the single-particle level. Large spin-orbit coupling and layer pseudospin texture are essential for generating the FQAHE in this system [17,18]. In contrast, the FQAHE was realized without these ingredients in rhombohedral graphene-hBN superlattices [19–21] when the conduction electrons were pushed *away* from the moiré interface by an external electric displacement field. Under these

*These authors contributed equally to this work.
†Contact author: longju@mit.edu
‡Contact author: ashoori@mit.edu

conditions, the superlattice potential is relatively weak, and there is considerable overlap between moiré conduction bands in the single-particle picture. Electronic interactions are therefore critical for isolating the topological miniband which hosts the FQAHE, triggering debate around its underlying origin in this material [22–27].

To shed light on this mystery, we study the opposite moiré-proximal case, when the displacement field pushes the conduction electrons toward the moiré interface. In this limit, the stronger superlattice potential may significantly modify the dispersion and topological structure of the minibands [28]. We address the moiré-proximal limit experimentally through capacitance measurements. While local compressibility probes, such as scanning single-electron transistors, can avoid defects and twist angle disorder, they generally do not allow for uniform and well-controlled displacement fields. Planar capacitance experiments, on the other hand, enable precise control over displacement field and are not hindered by tip gating effects. In addition, they provide quantitative measurements of gap widths and the thermodynamic density of states.

II. PHASE DIAGRAM OF R5G-hBN

We study a dual-gated device consisting of a sheet of rhombohedral pentalayer graphene encapsulated between two dielectric hBN layers (R5G-hBN). The graphene is crystallographically aligned to the hBN on the top side to produce a long-wavelength moiré superlattice potential. By tuning the effective top and bottom gate voltages V_t and V_b, we can independently control the electron density $n_e = (c_b V_b + c_t V_t)/e$ and applied perpendicular electric displacement field $D/\varepsilon_0 = (c_b V_b - c_t V_t)/2\varepsilon_0$, where c_t and c_b are the geometric capacitances per unit area from the top and bottom gates to the graphene. By applying an ac voltage excitation on the bottom gate and measuring the resultant current fluctuations on the top gate [Fig. 1(a)], we can determine the penetration capacitance c_p and hence the electronic compressibility $\partial n/\partial\mu$:

$$\frac{1}{c_p} = \frac{1}{c_t} + \frac{1}{c_b} + \frac{e^2}{c_t c_b}\left(\frac{\partial n}{\partial \mu}\right). \tag{1}$$

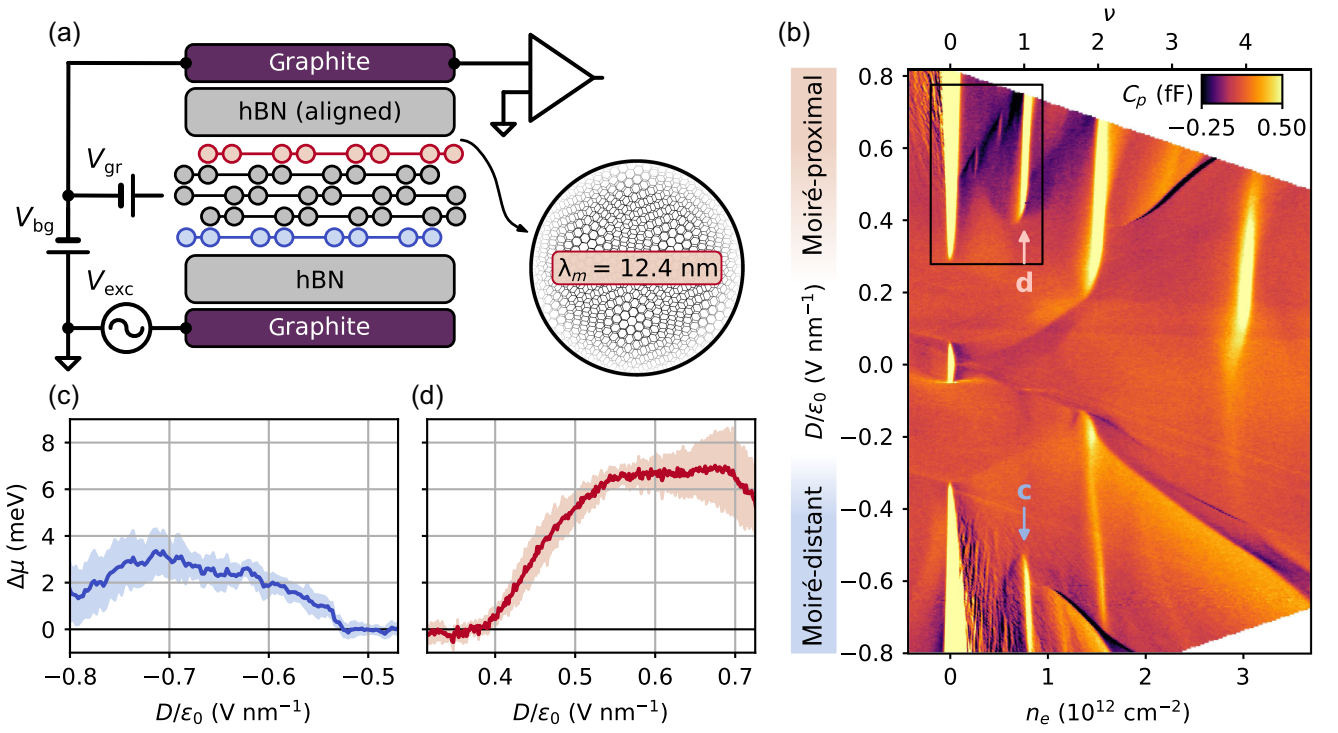

FIG. 1. Electronic compressibility of the rhombohedral pentalayer graphene superlattice. (a) Penetration capacitance measurement scheme. An ac excitation V_{exc} is applied to the bottom gate, and the penetrating signal is measured on the top gate. The effective top and bottom gate voltages are $V_t = -V_{gr}$ and $V_b = V_{bg} - V_{gr}$, respectively. A moiré superlattice forms at the interface between the top layer of graphene and the aligned hBN. (b) Map of penetration capacitance measured as a function of density and displacement field at 0 T. Bright features correspond to incompressible states. Vertical streaks appearing at the valence band edge for $D > 0$ and conduction band edge for $D < 0$ result from the formation of p-n junctions at the contacts, which lead to difficulties in the compressibility measurement [29]. The box in the upper left-hand corner corresponds to the area of focus in Figs. 2 and 3. (c), (d) Widths of the moiré-distant (c) and moiré-proximal (d) $\nu = 1$ gaps as a function of displacement field. A detailed analysis of the extraction of gap widths and error bands from the compressibility data is presented in Supplemental Material [30] (see also Ref. [31] therein).

Figure 1(b) shows the measured capacitance of an R5G-hBN device as a function of electron density and displacement field. The device has a moiré wavelength of 12.4 nm, corresponding to a twist angle of approximately 0.63°. We first focus on charge neutrality. Near $D/\varepsilon_0 = 0$, electronic correlations open a small gap, which closes with a moderate applied displacement field [32]. For $|D/\varepsilon_0| > 0.3$ V nm^{-1}, a single-particle gap grows with increasing D. Away from charge neutrality, vertical incompressible states correspond to integer fillings of the moiré superlattice. Figures 1(c) and 1(d) show the width of the $\nu = 1$ gap at 0 T for both signs of the displacement field as extracted from the compressibility data. The gap is significantly larger for positive D, consistent with the stronger lateral localization of electrons at the moiré interface. Similarly, we observe almost no gap at $\nu = 4$ for negative D, indicating a much weaker moiré potential experienced by electrons than at positive D [Fig. 1(b)]. Beyond the gaps at integer filling, the qualitative differences in the map for either sign of the displacement field indicate that the moiré band structure differs significantly between the two cases. From here on, we focus on the moiré-proximal positive D limit.

III. CORRELATIONS AND TOPOLOGY

In Fig. 2(a), we examine the electronic compressibility within the boxed region in Fig. 1(b). Beyond $D/\varepsilon_0 = 0.4$ V nm^{-1}, the system develops a gap at filling factor $\nu = 1$, and we measure enhanced compressibility between $\nu = 0$ and $\nu = 1$. Within this region, we observe a narrow stripe of negative compressibility [33–35] (where more charge enters the graphene than would be required to perfectly screen the applied ac excitation) moving diagonally from charge neutrality at $D/\varepsilon_0 = 0.5$ V nm^{-1} to the $\nu = 1$ gap at $D/\varepsilon_0 = 0.75$ V nm^{-1}. This stripe contains two prominent charge density waves (CDWs) at filling factors $\nu = 1/3$ and $\nu = 2/3$ along with weaker incompressible features developing around $\nu = 1/4$ and $\nu = 3/4$. Together, these phenomena indicate strong electronic correlations likely originating from a flat moiré band and a strong superlattice potential. In addition, as evidenced by the shift in density of the negative compressibility feature with D, the displacement field enables fine control over the dispersion of the moiré bands. To determine the topology of the $\nu = 1$ state, we study the density dependence of the $\nu = 1$ gap as a function of applied magnetic field [Fig. 2(b)]. We observe a $\mathcal{C} = -1$ state developing around 0.5 T, while a weaker trivial insulator emerges only above 2 T. Intriguingly, we measure a Chern number $\mathcal{C} = +1$ of opposite sign for the moiré-distant $\nu = 1$ state [36] (Supplemental Material Fig. S1 [30]), consistent with prior work in R5G-hBN [19].

The strong correlations and intrinsic topology present in the moiré-proximal limit are two key ingredients for the observation of FCIs at low magnetic field. A strong lattice potential can also stabilize topological charge density waves (TCDWs), also referred to as "symmetry-broken Chern insulators," with coexisting topological order and broken translational symmetry [37]. To search for these phenomena, we analyze the evolution of the compressibility within this band as a function of magnetic field. In the Hofstadter picture [38,39], gapped states evolve with field according to $n_e = tn_\Phi + sn_0$, where n_Φ is the magnetic flux density per unit cell and n_0 is the unit cell density. The Středa formula [40] then connects the slopes of these gaps to their associated Hall conductances through $\sigma_{xy} = te^2/h$. Figures 2(c) and 2(d) are Landau fans taken along the two lines indicated in Fig. 2(a). These fans display a variety of topological states that we characterize according to their inverse slope t and zero-field superlattice filling factor s.

We begin by noting the presence of the integer CI $(t, s) = (-1, 1)$ in both fans, although it is somewhat weaker at larger displacement field. FCI states occurring within this Chern band are expected to evolve with field as $(-\nu, \nu)$, where $0 < \nu < 1$. Indeed, we observe two such states, $(-1/3, 1/3)$ and $(-2/3, 2/3)$, in Fig. 2(d). In this map, we observe a transition between the $1/3$ FCI and a trivial CDW state below 2 T. As we increase the displacement field, this transition is pushed to lower magnetic field [Fig. 2(c)]. The persistence of the FCI down to 0.2 T demonstrates that the moiré conduction bands have favorable quantum geometry even in the presence of a strong superlattice potential. The FCI to CDW phase transition can be induced through tuning either the magnetic field or the displacement field. Thus, the nature of the correlated ground state is quite sensitive to external control parameters, making this system a useful platform for studying topological phase transitions. Finally, we identify additional states with integer t but fractional s, namely, $(-1, 1/2)$ and $(-1, 2/3)$, the aforementioned TCDWs. These states likely arise from commensurate charge density waves that distort the superlattice, doubling or tripling its unit cell. One of the filled subbands arising from this distortion then inherits the Chern number of the parent band [12].

The magnetic field dependence reveals a variety of fractional correlated phases. However, as is evident from the differences between Figs. 2(c) and 2(d), these states are quite sensitive to displacement field. We generically expect that changing the displacement field will alter both the band dispersion and the Berry curvature distribution, leading to topological phase transitions. To that end, we now study the compressibility between $\nu = 0$ and $\nu = 1$ as a function of displacement field at different magnetic fields. We start with the zero-field case as a reference [Figs. 3(a) and 3(b)], again noting the two prominent CDW states. Next, we turn to the 4 T case [Figs. 3(c) and 3(d)]. We observe the $\mathcal{C} = -1$ state with $(t, s) = (-1, 1)$ starting at $D/\varepsilon_0 = 0.3$ V nm^{-1}. As we increase the displacement field beyond $D/\varepsilon_0 = 0.65$ V nm^{-1}, the state terminates abruptly before reappearing very weakly above $D/\varepsilon_0 = 0.7$ V nm^{-1}. Simultaneously, we find that the topological states also disappear above $D/\varepsilon_0 = 0.65$ V nm^{-1}, with trivial CDWs taking their place.

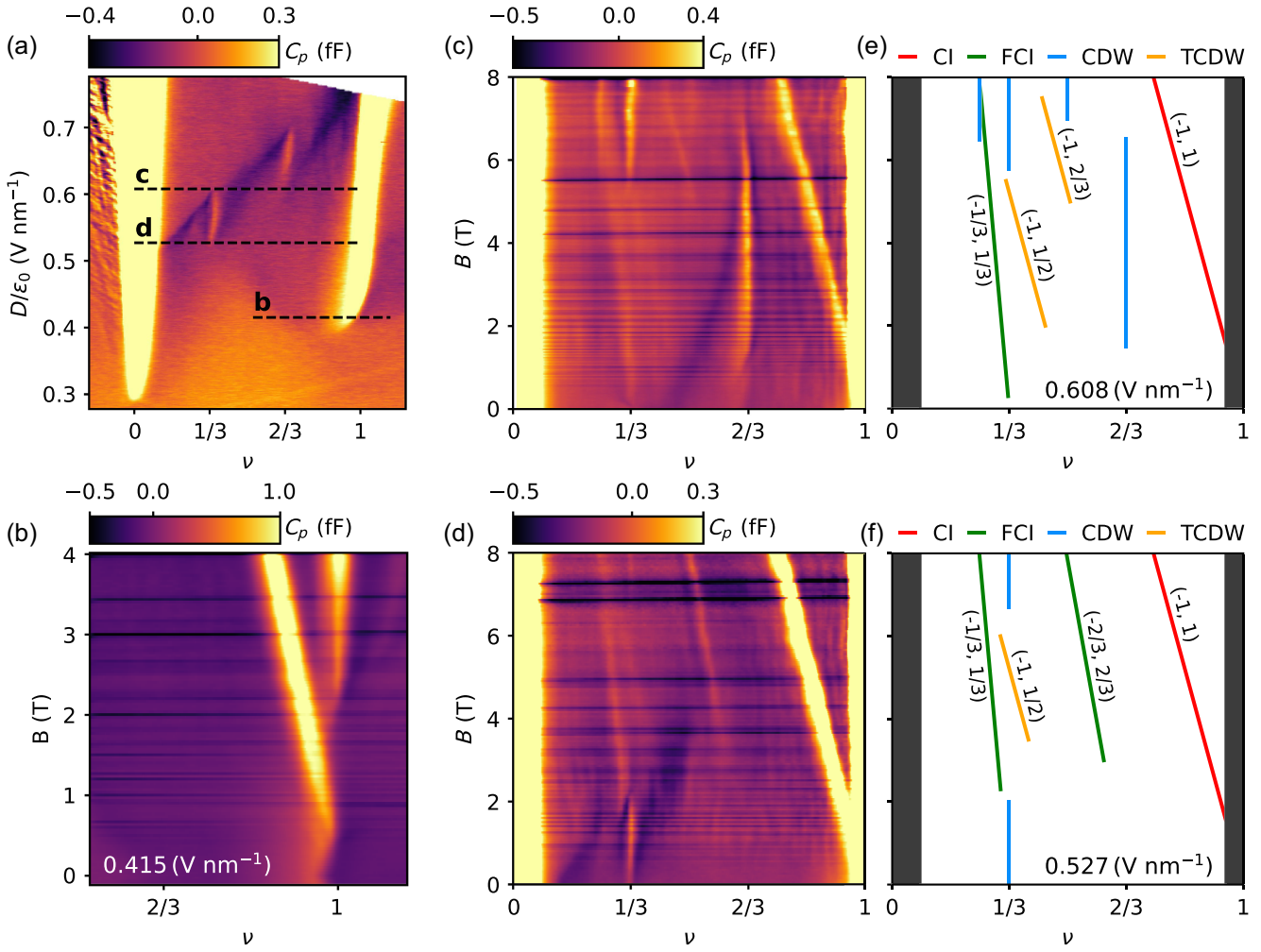

FIG. 2. Magnetic field dependence of correlated topological states. (a) High-resolution map of the compressibility between $\nu = 0$ and $\nu = 1$ on the moiré-proximal side, corresponding to the boxed region in Fig. 1(b). Dashed lines correspond to the Landau fans in (b)–(d). (b) Magnetic field dependence of the $\nu = 1$ state taken at $D/\epsilon_0 = 0.415$ V nm^{-1}. (c)–(f) Compressibility Landau fans taken at $D/\epsilon_0 = 0.608$ V nm^{-1} (c) and $D/\epsilon_0 = 0.527$ V nm^{-1} (d), with their schematic representations shown in (e) and (f), respectively. The dark horizontal bands in all Landau fans are due to cyclotron gaps that form in the graphite gates and decrease the total device capacitance. Other faint vertical features around 1 T in (c) and (d) do not trace back to filling factors with reasonably small denominators and we therefore do not assign them to fractional states. Incompressible states are colored according to their topological classification: red for Chern insulators, green for fractional Chern insulators, yellow for topological charge density waves, and blue for trivial charge density waves.

This pattern repeats at 8 T [Figs. 3(e) and 3(f)], with the FCI states vanishing along with the integer CI state at large D only to be replaced by CDWs. To summarize, we map out the displacement field-dependent ground state as a function of magnetic field for states with $s = 1/3$ and $s = 2/3$ [Figs. 3(g) and 3(h), respectively].

IV. CDW-FCI TRANSITION

The competition between the CDW and FCI states at $\nu = 1/3$ depends sensitively on the displacement field. To investigate this transition, we measure the compressibility at this filling factor over a narrow range of D [Figs. 4(a)–4(e)]. We also extract the energy gaps of both correlated states as a function of magnetic field [Fig. 4(l)]. In addition, we display a schematic phase diagram of this region in Fig. 4(k). We first differentiate between two regimes away from $\nu = 1/3$. In the upper-left and lower-right quadrants of the map, the system forms a highly compressible Fermi liquid. Adjacent to the CDW, we observe a stripe of negative compressibility where corresponding transport measurements show an enhanced in-plane resistivity (Supplemental Material Fig. S2 [30]). These two observations are consistent with a tentative assignment of this state to an incommensurate Wigner solid which, although pinned by defects, remains highly compressible as its density can change continuously. Right at $\nu = 1/3$, a highly incompressible state emerges out of the negative compressibility background as the system forms a CDW that is locked to the

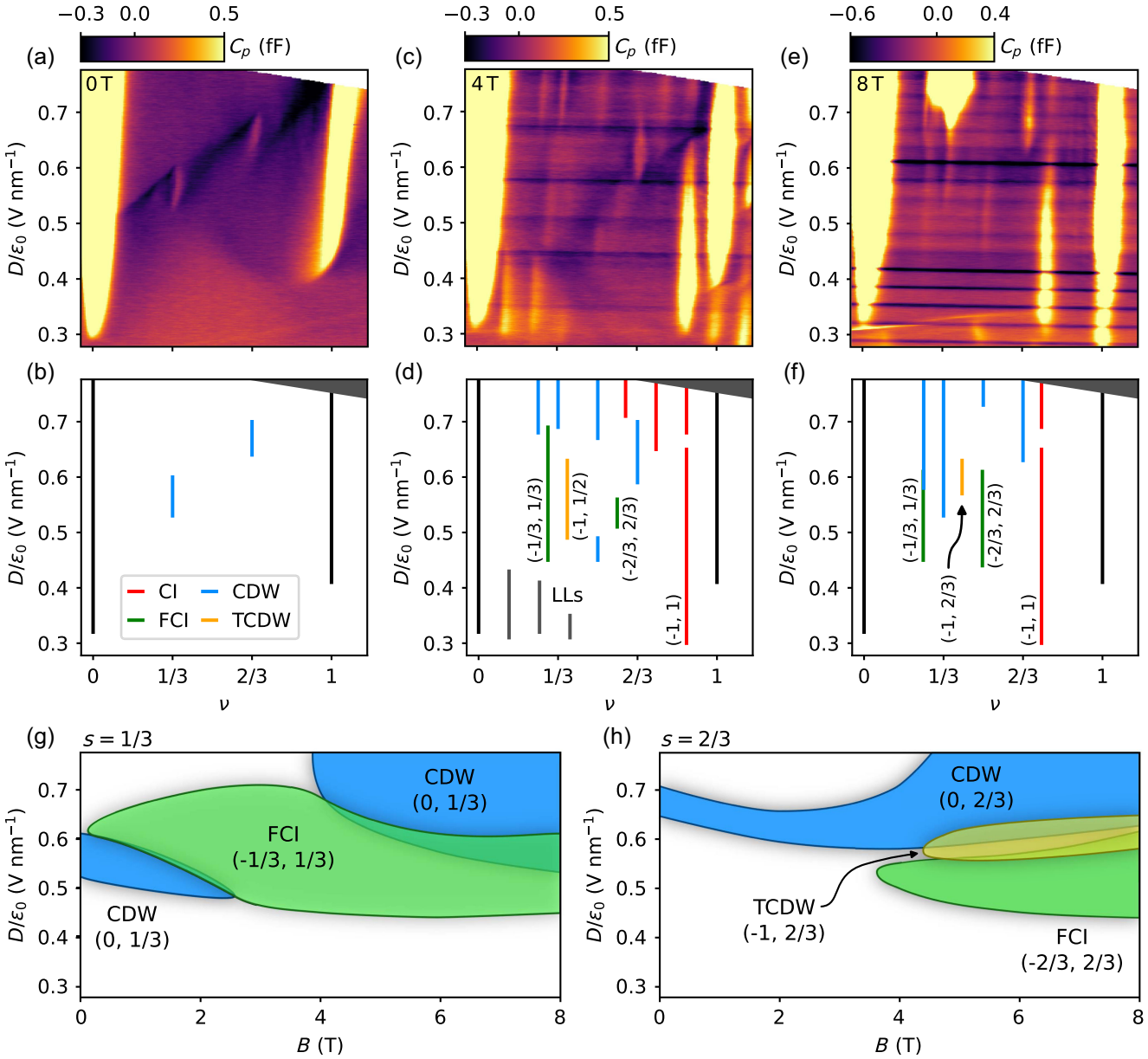

FIG. 3. Displacement field-driven topological phase transitions. (a)–(f) Penetration capacitance maps between $\nu = 0$ and $\nu = 1$ as a function of density and displacement field at 0 T (a), 4 T (c), and 8 T (e), corresponding to the boxed region in Fig. 1(b). Their schematic representations are shown in (b), (d), and (f), respectively, in which states are colored according to their topological classification. The dark horizontal bands are due to cyclotron gaps that form in the graphite gates and decrease the total device capacitance. Additional Landau levels (LLs) (indicated as gray in the schematic) appear near the conduction band edge in the bottom left-hand corner of the 4 T map. (g), (h) Phase diagrams in magnetic and displacement field of correlated states emerging out of $\nu = 1/3$ (g) and $\nu = 2/3$ (h). The numbers in parentheses label (t, s) for each state according to the Hofstadter model. Although the states overlap in displacement field, the individual phases occur at different densities for $B \neq 0$. Additional capacitance maps taken in 1 T intervals used to construct the phase diagrams are presented in Supplemental Material [30].

superlattice at a fixed charge density. The loss component [Figs. 4(f)–4(j)], which here increases with the graphene's in-plane resistance, shows a striking difference between the two correlated states at $\nu = 1/3$. The CDW produces a sharp peak in the loss; in contrast, there is no corresponding feature for the FCI. This is consistent with the real-space picture of these states. The CDW is locked in place and cannot move or slide easily, making it difficult to charge the sample on each ac cycle. The more delicate FCI, while incompressible, has lower resistance since it is not pinned to a lattice distortion.

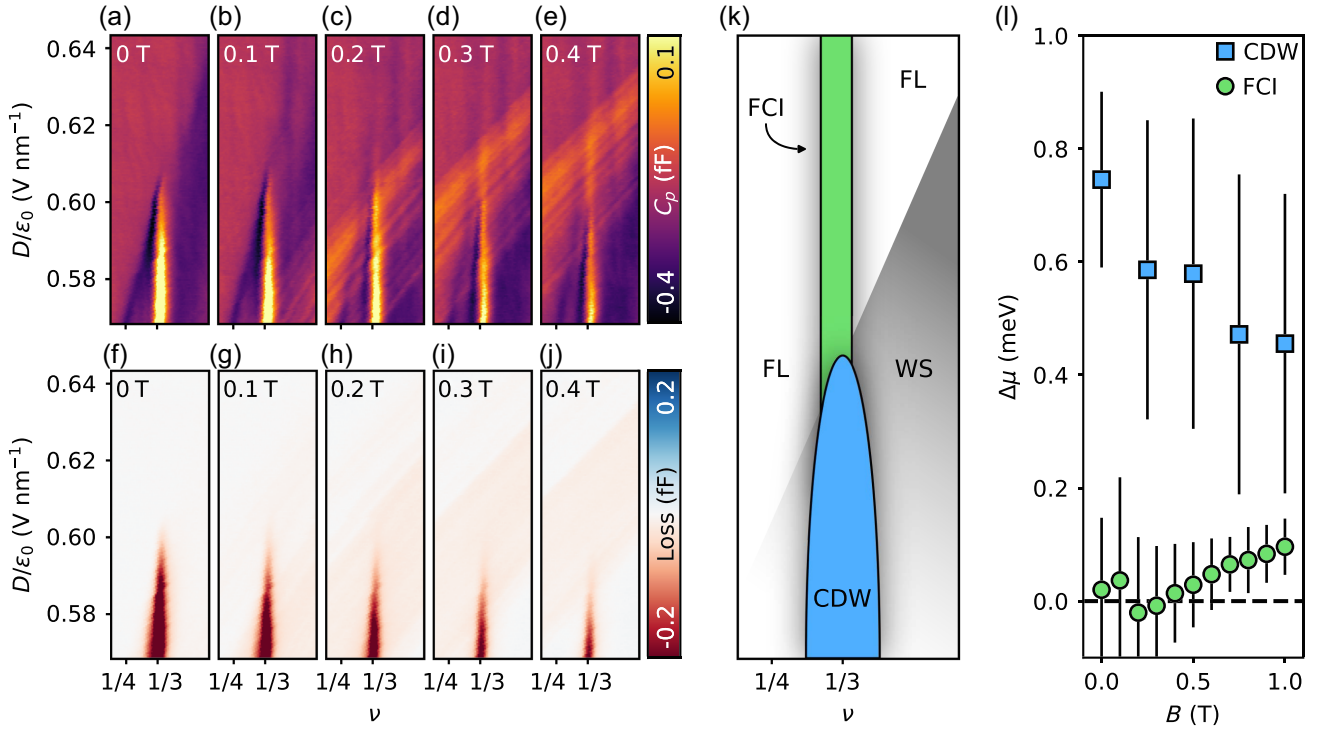

FIG. 4. CDW-FCI transition. (a)–(e) Evolution of the $\nu = 1/3$ CDW-FCI transition at low magnetic field. The FCI emerges as a faint vertical feature above the much brighter CDW at 0.2 T. The bright diagonal bands are measurement artifacts that occur at fixed voltages on the back gate. (f)–(j) Corresponding out-of-phase data for the plots in (a)–(e). (k) Schematic representation of the compressibility data, showing the locations of the Fermi liquid (FL), Wigner solid (WS), CDW, and FCI. (l) Widths of the CDW and FCI gaps as extracted from compressibility measurements on a different device with the same twist angle in which the diagonal banding is absent. For the CDW, we show the maximum values of the gap widths in Supplemental Material Fig. S3 [30]. For the FCI, we show the mean width of the gap between 0.618 and 0.640 V nm^{-1} in Supplemental Material Fig. S4 [30].

V. CONCLUSIONS

What accounts for the sensitivity of the correlated ground state to the displacement field? Rhombohedral multilayer graphene without a moiré superlattice already has a strongly displacement field-dependent band structure [41,42]. At the K points, the bottom of the conduction band flattens and then becomes dispersive again with increasing D [22,28]. With the addition of a superlattice potential, moiré minibands develop out of the flat region around the K points. These minibands inherit the displacement field dependence of the original unfolded bands, thus allowing us to modulate their bandwidths by tuning D [43,44]. Electronic interactions may then amplify this effect by further restructuring the minibands. On the moiré-distant side, this picture is consistent with the FQAHE or FCIs occurring over a narrow range of displacement field [19]. However, on the moiré-proximal side, the superlattice potential is strong enough to stabilize numerous CDWs in addition to FCI states.

Our observations stand in contrast to topological phase transitions seen in other graphene moiré systems [11,12]. In this experiment, the displacement field plays an outsized role in modulating the moiré bandwidth and Berry curvature, providing an additional experimental control for tuning between different correlated ground states. Our results demonstrate that intrinsic band topology and strong electronic correlations in R5G-hBN persist in a strong superlattice potential. In particular, we establish R5G-hBN as a unique platform to study FCIs in both the moiré-proximal and moiré-distant limit, providing a bridge between the recently reported FQAHE under a weak moiré potential and FCIs in other systems where the superlattice potential plays a dominant role.

Further opportunities for band structure engineering in this system include a systematic study of the effect of twist angle on the intricate correlated phase diagram. Also, recent theoretical work suggests that the moiré band topology may survive even as the superlattice potential becomes vanishingly weak [23,45]. This limit could be probed experimentally by imprinting a superlattice potential onto the pentalayer with a separate moiré heterostructure or patterned substrate [23,46–50].

VI. METHODS

A. Device fabrication

The pentalayer graphene and hBN flakes were prepared by mechanical exfoliation onto SiO_2-Si substrates. The rhombohedral domains of pentalayer graphene were

identified and confirmed using IR camera, near-field infrared microscopy, and Raman spectroscopy and isolated by cutting with a femtosecond laser. The van der Waals heterostructure was made following a dry transfer procedure. We picked up the top hBN, graphite, middle hBN, and the pentalayer graphene using polypropylene carbonate film and landed it on a prepared bottom stack consisting of an hBN and graphite bottom gate. We aligned the long straight edge of graphene to that of hBN to nearly zero degrees to create a large moiré superlattice. The device was then etched into a multiterminal structure using standard *e*-beam lithography and reactive-ion etching. We deposited Cr-Au for electrical connections to the source, drain, and gate electrodes.

B. Compressibility measurements

All compressibility measurements in this work were performed in an Oxford Instruments Heliox ^{3}He refrigerator with a base temperature of 300 mK. The sample impedance is measured against a ∼25 fF reference in an impedance bridge circuit (Supplemental Material Fig. S5 [30]). At the beginning of each measurement, independent ac excitations are applied to the sample and reference to null the signal on the balance point of the bridge. As the sample impedance changes, the new impedance can be computed from the resulting off-balance voltage on the balance point. In order to reliably measure the off-balance signal, a cryogenic amplifier [51] is placed at the balance point of the bridge, which significantly reduces the output impedance of the circuit. Without this amplifier, the signal would be lost to the comparatively large parasitic capacitance of the coaxial cabling on the output line. At room temperature, the signal is recovered with a Stanford Research Systems SR865a lock-in amplifier. The ac excitations applied to the sample have an rms amplitude of 10 mV and a frequency of either 10 kHz [Figs. 1, 2(a), and 3] or 150 kHz [Figs. 2(b)–2(d) and 4].

ACKNOWLEDGMENTS

We acknowledge helpful discussions with Liang Fu, Senthil Todadri, and Trithep Devakul. Compressibility measurements were supported by the STC Center for Integrated Quantum Materials, NSF Grant No. DMR-1231319. L. J. acknowledges support from a Sloan Fellowship. S. H. A. was supported by the NSF Graduate Research Fellowship under Grant No. 1122374. The device fabrication of this study was supported by the U.S. Department of Energy, Office of Science, Basic Energy Sciences, Materials Sciences and Engineering Division under Grant No. DE-SC0025325.

DATA AVAILABILITY

The data that support the findings of this article are openly available [52].

[1] K. v. Klitzing, G. Dorda, and M. Pepper, *New method for high-accuracy determination of the fine-structure constant based on quantized Hall resistance*, Phys. Rev. Lett. **45**, 494 (1980).
[2] D. C. Tsui, H. L. Stormer, and A. C. Gossard, *Two-dimensional magnetotransport in the extreme quantum limit*, Phys. Rev. Lett. **48**, 1559 (1982).
[3] F. D. M. Haldane, *Model for a quantum Hall effect without Landau levels: Condensed-matter realization of the "parity anomaly"*, Phys. Rev. Lett. **61**, 2015 (1988).
[4] E. Tang, J.-W. Mei, and X.-G. Wen, *High-temperature fractional quantum Hall states*, Phys. Rev. Lett. **106**, 236802 (2011).
[5] K. Sun, Z. Gu, H. Katsura, and S. Das Sarma, *Nearly flatbands with nontrivial topology*, Phys. Rev. Lett. **106**, 236803 (2011).
[6] T. Neupert, L. Santos, C. Chamon, and C. Mudry, *Fractional quantum Hall states at zero magnetic field*, Phys. Rev. Lett. **106**, 236804 (2011).
[7] D. N. Sheng, Z.-C. Gu, K. Sun, and L. Sheng, *Fractional quantum Hall effect in the absence of Landau levels*, Nat. Commun. **2**, 389 (2011).
[8] N. Regnault and B. A. Bernevig, *Fractional Chern insulator*, Phys. Rev. X **1**, 021014 (2011).
[9] S. A. Parameswaran, R. Roy, and S. L. Sondhi, *Fractional quantum Hall physics in topological flat bands*, C.R. Phys. **14**, 816 (2013).
[10] E. J. Bergholtz and Z. Liu, *Topological flat band models and fractional Chern insulators*, Int. J. Mod. Phys. B **27**, 1330017 (2013).
[11] E. M. Spanton, A. A. Zibrov, H. Zhou, T. Taniguchi, K. Watanabe, M. P. Zaletel, and A. F. Young, *Observation of fractional Chern insulators in a van der Waals heterostructure*, Science **360**, 62 (2018).
[12] Y. Xie, A. T. Pierce, J. M. Park, D. E. Parker, E. Khalaf, P. Ledwith, Y. Cao, S. H. Lee, S. Chen, P. R. Forrester, K. Watanabe, T. Taniguchi, A. Vishwanath, P. Jarillo-Herrero, and A. Yacoby, *Fractional Chern insulators in magic-angle twisted bilayer graphene*, Nature (London) **600**, 439 (2021).
[13] J. Cai, E. Anderson, C. Wang, X. Zhang, X. Liu, W. Holtzmann, Y. Zhang, F. Fan, T. Taniguchi, K. Watanabe, Y. Ran, T. Cao, L. Fu, D. Xiao, W. Yao, and X. Xu, *Signatures of fractional quantum anomalous Hall states in twisted* $MoTe_2$, Nature (London) **622**, 63 (2023).
[14] Y. Zeng, Z. Xia, K. Kang, J. Zhu, P. Knüppel, C. Vaswani, K. Watanabe, T. Taniguchi, K. F. Mak, and J. Shan, *Thermodynamic evidence of fractional Chern insulator in moiré* $MoTe_2$, Nature (London) **622**, 69 (2023).
[15] F. Xu, Z. Sun, T. Jia, C. Liu, C. Xu, C. Li, Y. Gu, K. Watanabe, T. Taniguchi, B. Tong, J. Jia, Z. Shi, S. Jiang, Y. Zhang, X. Liu, and T. Li, *Observation of integer and fractional quantum anomalous Hall effects in twisted bilayer* $MoTe_2$, Phys. Rev. X **13**, 031037 (2023).
[16] H. Park, J. Cai, E. Anderson, Y. Zhang, J. Zhu, X. Liu, C. Wang, W. Holtzmann, C. Hu, Z. Liu, T. Taniguchi, K. Watanabe, J.-H. Chu, T. Cao, L. Fu, W. Yao, C.-Z. Chang, D. Cobden, D. Xiao, and X. Xu, *Observation of fractionally quantized anomalous Hall effect*, Nature (London) **622**, 74 (2023).

[17] F. Wu, T. Lovorn, E. Tutuc, I. Martin, and A. H. MacDonald, *Topological insulators in twisted transition metal dichalcogenide homobilayers*, Phys. Rev. Lett. **122**, 086402 (2019).

[18] T. Devakul, V. Crépel, Y. Zhang, and L. Fu, *Magic in twisted transition metal dichalcogenide bilayers*, Nat. Commun. **12**, 6730 (2021).

[19] Z. Lu, T. Han, Y. Yao, A. P. Reddy, J. Yang, J. Seo, K. Watanabe, T. Taniguchi, L. Fu, and L. Ju, *Fractional quantum anomalous Hall effect in multilayer graphene*, Nature (London) **626**, 759 (2024).

[20] J. Xie, Z. Huo, X. Lu, Z. Feng, Z. Zhang, W. Wang, Q. Yang, K. Watanabe, T. Taniguchi, K. Liu, Z. Song, X. C. Xie, J. Liu, and X. Lu, *Tunable fractional Chern insulators in rhombohedral graphene superlattices*, arXiv: 2405.16944.

[21] Y. Choi, Y. Choi, M. Valentini, C. L. Patterson, L. F. W. Holleis, O. I. Sheekey, H. Stoyanov, X. Cheng, T. Taniguchi, K. Watanabe, and A. F. Young, *Superconductivity and quantized anomalous Hall effect in rhombohedral graphene*, Nature (London) **639**, 342 (2025).

[22] Z. Dong, A. S. Patri, and T. Senthil, *Theory of fractional quantum anomalous Hall phases in pentalayer rhombohedral graphene moiré structures*, Phys. Rev. Lett. **133**, 206502 (2023).

[23] B. Zhou, H. Yang, and Y.-H. Zhang, *Fractional quantum anomalous Hall effect in rhombohedral multilayer graphene in the moiréless limit*, Phys. Rev. Lett. **133**, 206504 (2024).

[24] J. Dong, T. Wang, T. Wang, T. Soejima, M. P. Zaletel, A. Vishwanath, and D. E. Parker, *Anomalous Hall crystals in rhombohedral multilayer graphene. I. Interaction-driven Chern bands and fractional quantum Hall states at zero magnetic field*, Phys. Rev. Lett. **133**, 206503 (2024).

[25] Y. H. Kwan, J. Yu, J. Herzog-Arbeitman, D. K. Efetov, N. Regnault, and B. A. Bernevig, *Moiré Fractional Chern insulators III: Hartree-Fock phase diagram, magic angle regime for Chern insulator states, the role of the moiré potential and Goldstone gaps in rhombohedral graphene superlattices*, arXiv:2312.11617 [Phys. Rev. B (to be published)].

[26] Z. Guo, X. Lu, B. Xie, and J. Liu, *Fractional Chern insulator states in multilayer graphene moiré superlattices*, Phys. Rev. B **110**, 075109 (2024).

[27] K. Huang, X. Li, S. Das Sarma, and F. Zhang, *Self-consistent theory of fractional quantum anomalous Hall states in rhombohedral graphene*, Phys. Rev. B **110**, 115146 (2024).

[28] Y.-H. Zhang, D. Mao, Y. Cao, P. Jarillo-Herrero, and T. Senthil, *Nearly flat Chern bands in moiré superlattices*, Phys. Rev. B **99**, 075127 (2019).

[29] H. Zhou, T. Xie, A. Ghazaryan, T. Holder, J. R. Ehrets, E. M. Spanton, T. Taniguchi, K. Watanabe, E. Berg, M. Serbyn, and A. F. Young, *Half- and quarter-metals in rhombohedral trilayer graphene*, Nature (London) **598**, 429 (2021).

[30] See Supplemental Material at http://link.aps.org/supplemental/10.1103/75gl-jzl6 for additional compressibility and transport measurements, statistical fits to features in Landau fans, circuit diagrams, and a discussion on extracting gap widths from capacitance data.

[31] S. C. Dultz and H. W. Jiang, *Thermodynamic signature of a two-dimensional metal-insulator transition*, Phys. Rev. Lett. **84**, 4689 (2000).

[32] T. Han, Z. Lu, G. Scuri, J. Sung, J. Wang, T. Han, K. Watanabe, T. Taniguchi, H. Park, and L. Ju, *Correlated insulator and Chern insulators in pentalayer rhombohedral-stacked graphene*, Nat. Nanotechnol. **19**, 181 (2024).

[33] M. Bello, E. Levin, B. Shklovskii, and A. L. Efros, *Density of localized states in the surface band of a metal-insulator-semiconductor structure*, Zh. Eksp. Teor. Fiz. **53**, 822 (1981).

[34] B. Tanatar and D. M. Ceperley, *Ground state of the two-dimensional electron gas*, Phys. Rev. B **39**, 5005 (1989).

[35] J. P. Eisenstein, L. N. Pfeiffer, and K. W. West, *Negative compressibility of interacting two-dimensional electron and quasiparticle gases*, Phys. Rev. Lett. **68**, 674 (1992).

[36] T. Tan and T. Devakul, *Parent Berry curvature and the ideal anomalous Hall crystal*, Phys. Rev. X **14**, 041040 (2024).

[37] L. Wang, Y. Gao, B. Wen, Z. Han, T. Taniguchi, K. Watanabe, M. Koshino, J. Hone, and C. R. Dean, *Evidence for a fractional fractal quantum Hall effect in graphene superlattices*, Science **350**, 1231 (2015).

[38] D. R. Hofstadter, *Energy levels and wave functions of Bloch electrons in rational and irrational magnetic fields*, Phys. Rev. B **14**, 2239 (1976).

[39] D. J. Thouless, M. Kohmoto, M. P. Nightingale, and M. den Nijs, *Quantized Hall conductance in a two-dimensional periodic potential*, Phys. Rev. Lett. **49**, 405 (1982).

[40] P. Streda, *Theory of quantised Hall conductivity in two dimensions*, J. Phys. C **15**, L717 (1982).

[41] M. Koshino and E. McCann, *Trigonal warping and Berry's phase $N\pi$ in ABC-stacked multilayer graphene*, Phys. Rev. B **80**, 165409 (2009).

[42] T. Han, Z. Lu, G. Scuri, J. Sung, J. Wang, T. Han, K. Watanabe, T. Taniguchi, L. Fu, H. Park, and L. Ju, *Orbital multiferroicity in pentalayer rhombohedral graphene*, Nature (London) **623**, 41 (2023).

[43] B. L. Chittari, G. Chen, Y. Zhang, F. Wang, and J. Jung, *Gate-tunable topological flat bands in trilayer graphene boron-nitride moiré superlattices*, Phys. Rev. Lett. **122**, 016401 (2019).

[44] Y. Park, Y. Kim, B. L. Chittari, and J. Jung, *Topological flat bands in rhombohedral tetralayer and multilayer graphene on hexagonal boron nitride moiré superlattices*, Phys. Rev. B **108**, 155406 (2023).

[45] J. Dong, T. Wang, T. Wang, T. Soejima, M. P. Zaletel, A. Vishwanath, and D. E. Parker, *Anomalous Hall crystals in rhombohedral multilayer graphene I: Interaction-driven Chern bands and fractional quantum Hall states at zero magnetic field*, Phys. Rev. Lett. **133**, 206503 (2024).

[46] Y. Xu, C. Horn, J. Zhu, Y. Tang, L. Ma, L. Li, S. Liu, K. Watanabe, T. Taniguchi, J. C. Hone, J. Shan, and K. F. Mak, *Creation of moiré bands in a monolayer semiconductor by spatially periodic dielectric screening*, Nat. Mater. **20**, 645 (2021).

[47] Sayed Ali Akbar Ghorashi, A. Dunbrack, A. Abouelkomsan, J. Sun, X. Du, and J. Cano, *Topological and stacked flat bands in bilayer graphene with a superlattice potential*, Phys. Rev. Lett. **130**, 196201 (2023).

[48] Z. Zhang, J. Xie, W. Zhao, R. Qi, C. Sanborn, S. Wang, S. Kahn, K. Watanabe, T. Taniguchi, A. Zettl, M. Crommie, and F. Wang, *Engineering correlated insulators in bilayer graphene with a remote Coulomb superlattice*, Nat. Mater. **23**, 189 (2024).

[49] D. S. Kim *et al.*, *Electrostatic moiré potential from twisted hexagonal boron nitride layers*, Nat. Mater. **23**, 65 (2024).

[50] X. Wang, C. Xu, S. Aronson, D. Bennett, N. Paul, P. J. D. Crowley, C. Collignon, K. Watanabe, T. Taniguchi, R. Ashoori, E. Kaxiras, Y. Zhang, P. Jarillo-Herrero, and K. Yasuda, *Band structure engineering using a moiré polar substrate*, Nat. Commun. **16**, 178 (2025).

[51] G. A. Steele, *Imaging transport resonances in the quantum Hall effect*, Ph.D. thesis, MIT, 2006.

[52] S. H. Aronson, *Data for Displacement field-controlled fractional Chern insulators and charge density waves in a graphene/hBN moire superlattice*, Zenodo, 10.5281/zenodo.15732368 (2025).